A comparison of the ECMWF forecast model with observations over the annual cycle at SHEBA.

C. S. Bretherton[1], S. R. de Roode[1], C. Jakob[2], E. L Andreas[3], J. Intrieri[4], and R. E. Moritz[5], and P. Ola G. Persson[4,6]

Submitted 2 December 1999
Revised 26 May 2000

Journal of Geophysical Research,
FIRE Arctic Clouds Experiment Special Issue

---

[1]*Department of Atmospheric Sciences, University of Washington, Seattle WA*

[2]*ECMWF, Reading, England*

[3]*CRREL, Hanover, NH*

[4]*NOAA Environmental Technology Laboratory, Boulder CO*

[5]*Applied Physics Laboratory, University of Washington, Seattle WA*

[6]*University of Colorado/CIRES, Boulder CO*

Corresponding author address:

Christopher S. Bretherton, Department of Atmospheric Sciences, University of Washington, Box 351640, Seattle, WA, 98195-1640. Email: breth@atmos.washington.edu.

Abstract

A central objective of the Surface Heat Budget of the Arctic Ocean (SHEBA) experiment was to provide a comprehensive observational test for single-column models of the atmosphere-sea ice-ocean system over the Arctic Ocean. For single-column modeling, one must specify the time-varying tendencies due to horizontal and vertical advection of air through the column. Due to the difficulty of directly measuring these tendencies, it was decided for SHEBA to obtain them from short-range forecasts of the European Centre for Medium-Range Weather Forecasts (ECMWF) global forecast model, into which SHEBA rawinsonde and surface synoptic observations were routinely assimilated. The quality of these forecasts directly affects the reliability of the derived advective tendencies. In addition, the ECMWF-forecast thermodynamic and cloud fields, and radiative and turbulent fluxes present an illuminating comparison of the SHEBA observations with a state-of-the-art global numerical model.

The authors compare SHEBA soundings, cloud and boundary layer observations with the ECMWF model output throughout the SHEBA year. They find that above the boundary layer, the model was faithful to the SHEBA rawinsonde observations and maintained a proper long-term balance between advective and nonadvective tendencies of heat and moisture. This lends credence to use of the ECMWF-predicted advective tendencies for single-column modeling studies.

The model-derived cloud properties and precipitation (which were not assimilated from observations) are compared with cloud radar, lidar, microwave radiometer, surface turbulent and radiative measurements, and basic surface meteorology. The model's slab sea-ice model led to large surface temperature errors and insufficient synoptic variability of temperature. The overall height distribution of cloud was fairly well simulated (though somewhat overestimated) in all seasons, as was precipitation. However, the model clouds typically had a much higher ratio of cloud ice to cloud water than suggested by lidar depolarization measurements, and a smaller optical depth, leading to monthly biases of up to 50 W m^{-2} in the monthly surface downwelling longwave and shortwave radiation. Further biases in net radiation were due to the inaccurate model assumption of constant surface albedo.

Observed turbulent sensible and latent heat fluxes tended to be small throughout SHEBA. During high-wind periods during the winter, the ECMWF model predicted sustained downward heat fluxes of up to 60 W m^{-2}, much higher than observed. A detailed comparison suggests that this error was due to both inadequate resolution of the 31-level model and a deficient parameterization of sea-ice thermodynamics.

1. Introduction

A central objective of the Surface Heat Budget of the Arctic Ocean (SHEBA) experiment was to provide a comprehensive observational test for single-column models of the atmosphere-sea ice-ocean system over the Arctic Ocean. One crucial boundary condition for such models is the time-varying tendencies of heat and moisture from horizontal and vertical advection. Due to the difficulty of directly obtaining these tendencies, SHEBA and FIRE.ACE (the First International Satellite Cloud Climatology Regional Experiment Arctic Cloud Experiment) chose to specify them based on analyses from operational forecast models. The European Centre for Medium-Range Weather Forecasts (ECMWF) cooperated closely with FIRE.ACE and SHEBA to provide model predictions of these tendencies from the ECMWF global weather forecast model, version CY18R6, run with 31 vertical levels (6 below 850 mb) and T_L319 spectral resolution (nominal 60 km grid spacing). Model predictions were output for every hour. To reduce initialization transients in the model velocity fields (especially vertical velocity), all ECMWF model output was based on 12-35 hour forecasts. To provide the best possible analysis around the SHEBA ice station, twice-daily SHEBA rawinsonde ascents (four times daily during 1 Apr. - 7 Jun. 1998 and a few days in July 1998) and hourly surface air pressure were routinely assimilated into the forecast model (with almost no data rejection) over the period 22 Oct. 1997-30 Sep. 1998.

The first goal of this paper is to assess the quality of the ECMWF analysis by comparing the model output for the SHEBA column with the SHEBA observations. The second goal of this paper is to look at how some physical parameterizations within the ECMWF model performed. This is of relevance to SHEBA and FIRE since most of the physical parameterizations used by ECMWF are at least as advanced as those in most general circulation models. The forecast model was constantly adjusted to the observed thermodynamic state of the atmosphere by assimilation of the soundings and surface observations, but clouds, precipitation, radiative and turbulent fluxes are only indirectly constrained, so can usefully be compared with observations.

This paper is a sequel to the work of Beesley et al. (2000; hereafter B00), who compared SHEBA observations of clouds, precipitation, radiative and turbulent fluxes during Nov.-Dec. 1997

(early winter) with the ECMWF model output. Their three principal findings were: First, the ECMWF model produced a reasonable depiction of the role of clouds, including a time-height distribution of cloud and precipitation that agreed fairly well with the SHEBA mm-wave cloud radar, and good predictions of downwelling longwave radiation at the surface. However, SHEBA lidar depolarization measurements suggested that the model appeared to underestimate the frequency of cloud layers primarily composed of supercooled water. Second, the sea-ice model, which treated sea-ice as an isothermal slab, dramatically damped day-to-day surface air temperature fluctuations compared to observations, creating 10-15 K errors in surface air temperature, particularly under clear calm conditions. Third, despite good forecasts of near-surface winds, the model produced extended periods of downward surface turbulent heat fluxes as large as 50 W m^{-2}, while observations showed turbulent heat fluxes rarely got even a tenth this large.

In this paper, we extend this analysis to the full annual cycle, including model performance during the spring and summer season when FIRE-ACE aircraft measurements were taking place. In additions to the data sources used by B00, we also compare shortwave radiation, microwave radiometer data, and precipitation to the model, and use final, rather than preliminary versions of the datasets. Our study corroborates and extends the principal conclusions of B00; we hope that it can serve as a more authoritative benchmark for the testing of other forecast and single-column atmospheric models against the SHEBA dataset. Many of the observations used for this study have time or vertical resolution too fine to be convenient for analyses of the full annual cycle and were reduced to a more compact hourly or daily-averaged form. The datasets used in this study are summarized in Table 1, and can be requested by email from the lead author.

In Section 2, we compare the model and observed soundings, surface pressure and winds, and thermodynamic budgets to assess the consistency of the model output with the observations it assimilated. In Section 3, we look at surface turbulent fluxes, and in Section 4 we compare cloud properties. Section 5 discusses the strengths and weaknesses of the model, and possible general ramifications for Arctic climate modeling.

2. Basic Thermodynamic Structure

One might hope that deviations of model predictions from the assimilated observations should be fairly small (keeping in mind possible error growth and the downstream advection of the assimilated effects of ice station data away from the SHEBA location during the 12-35 hour forecast period). In this section we quantify these deviations, and those of some other basic thermodynamic variables. We start by comparing surface variables observed by the SHEBA Atmospheric Surface Flux Group (ASFG).

The rms model - observation difference in daily averaged surface air pressure was slightly over 1 mb, very small compared to the 50 mb range of daily average surface air pressure over the SHEBA year (not shown). Hourly averages of 10 m wind, 2.5 m temperature and humidity were calculated as long as at least four 10-minute periods during the hour contained two or more minutes of good data, and the airflow was not directly from the ship or through the tower. The temperature measurements were interpolated to 2.5 m from the available sensor heights of the ASFG flux tower. After 1 Aug.1998, ice melt beneath the tower left the lowest temperature sensor slightly above 2.5 m above ground level, so we used just data from the sensor as a proxy for 2.5 m temperature We then aggregated this data into daily averages for comparison with the ECMWF model. As found by B00, surface (10 m) winds, though not assimilated, were also quite accurately forecast, even when the PBL was quite stable (not shown). However, the near-surface air temperature errors associated with the ECMWF slab ice model that were found by B00 continued through the winter (Fig. 1a). Even in summer, when the ice surface was melting and essentially isothermal both in the ECMWF model and observations, the model had a surface cold bias (Fig. 1b) since the melting temperature of the sea-ice surface was wrongly assumed to be equal to the freezing point of sea water (-1.8 C).

Now, we turn to the vertical thermodynamic structure. Until 29 Jun. 1998, the ECMWF model only assimilated thicknesses and vertically averaged mixing ratios between the standard rawinsonde pressure levels, and the winds at the standard pressure levels (after this time significant-level rawinsonde data was used) . Thus one cannot expect fine-scale vertical structures in the temper-

ature and humidity fields to be faithful to the observations. Fig. 2 shows the distribution of differences between the rawinsonde and model-predicted temperature and relative humidity (with respect to liquid water) for Apr. 1998, a period typical of all the cold-season months we have examined. All 00 and 12 UTC SHEBA rawinsonde soundings for the month were used, except for two which were visually judged to be unreasonable. The standard deviation of the temperature difference was fairly small (2 K), with little bias above 900 mb. The model-predicted temperatures had a high bias below 900 mb, reaching a maximum near the surface. This is a manifestation of the large thermal inertia of the slab ice model, which prevented near-surface air temperatures from cooling nearly as much was observed during a cold period in the last third of April.

The model relative humidity is quite scattered about the observations, showing the low weight placed on rawinsonde humidity estimates by the data assimilation system. This suggests that the moisture field and the moisture advection in the model may be less trustworthy than for temperature. However, some of the model-sonde discrepancies may be due to mesoscale variability and fine structure in the relative humidity field that show up in a point sounding, but are not representative of an areal average. Generally, the ECMWF column-averaged water vapor path agreed with the sondes quite well. For example, Fig. 3 shows the comparison for April 1998, along with water vapor path independently retrieved from the upward-looking microwave radiometer at the SHEBA ship (the latter is discussed further in Section 4d).

A last important check on the model performance is to examine the self-consistency of its budgets of heat and moisture. In an ideal forecast model, the model-computed tendencies of temperature and moisture will always match their observed tendencies. If model forecasts systematically drift away from the observations, the model will have unbalanced heat and moisture budgets in which the predicted and observed tendencies are systematically different. Such drift may be associated with (or rapidly lead to) systematic errors in the velocity field and the advective tendencies, which would render these tendencies less useful for forcing single-column models. One method of assessing the relative importance of such systematic drifts is to separately compute the 'adiabatic' (advective) tendencies and nonadiabatic tendencies (i.e. due to physical parameteriza-

tions) of heat and moisture. Fig. 4 shows the adiabatic and nonadiabatic tendencies of temperature and moisture in the SHEBA column for Jan. 1998. If the ECMWF model had no systematic drift during the 12-35 hour forecast period, these would sum to the observed monthly mean tendencies of T and q, which were negligibly small by comparison. Reassuringly, the adiabatic and nonadiabatic tendencies of temperature and moisture in the ECMWF model do very nearly balance at all levels in Jan. 1998, and in fact in all SHEBA months.

3. Turbulent Fluxes

Turbulent sensible heat fluxes were measured by the ASFG using sonic anemometers on the SHEBA flux tower at five different levels. Hourly covariance estimates of fluxes were computed by using a Fast Fourier Transform technique on 13.6 minutes of detrended data sampled at 10 Hz. The spectra from 5 such overlapping periods were combined for the hourly flux values. The fluxes were computed as long as 27.2 consecutive minutes of data were available during the hour. Sensor intercomparisons were done throughout the year. In this paper, we used the median of the fluxes from all levels available for a given hour. We interpolated the tower profiles of temperature to 2.5 m, and wind to 10 m.

Fig. 5 compares observed daily-averaged turbulent heat fluxes for Jan.-Mar. 1998 with those predicted by the ECMWF model. Several periods of excessively large downward heat fluxes, sometimes lasting more than two days, are predicted by the model . During the summer analogous errors are not observed; both the ECMWF and observed surface sensible heat fluxes are almost always less than 5 W m^{-2} in magnitude. One might be tempted to attribute the anomalous heat fluxes to the erroneous surface temperatures, which when coupled to assimilated rawinsonde observations will skew the PBL stability. In fact, Viterbo et al. (1999) demonstrated that the surface temperature response, in their case to soil water freezing, can strongly interact with the evolution of the stable boundary layer. However, we will argue in this section that these periods may also reflect insufficient model vertical resolution to handle the dynamics of a stable boundary layer in high winds.

We examined several of the high-flux events in detail. These periods were characterized by warm advection and high near-surface winds of 15 m s^{-1}. Fig. 6a compares observed and model potential temperature soundings at 11:15 UTC on 21 Feb. 1998 (Julian Day 417.5 on Fig. 5). Their gross shape was similar, but the observations showed a shallow, shear-driven, nearly well-mixed layer capped by a sharp inversion at $\sigma = p/p_{surf} = 0.97$. The model smeared this profile out into a more uniform stable low-level stratification, presumably due to insufficient resolution. Fig. 6b shows the model and observed wind and turbulent heat flux profiles. The model and observed wind profiles are similar. However, there are significant downward turbulent heat fluxes in the model up to $\sigma = 0.91$, while the observed sharp inversion suggests that in reality, turbulent mixing did not extend above $\sigma = 0.97$. The model surface turbulent heat flux was -60 W m^{-2}; the observed surface heat flux was only half as large at this time. One contributor to the large modelled heat fluxes may be the ECMWF vertical diffusion parameterization, which does not have a Richardson number cutoff, and produces turbulent mixing even in the highly stable stratification (gradient Richardson numbers of 1-8) of the deep modelled shear layer. In Oct. 1999, the vertical resolution of the ECMWF forecast model was doubled (60 vertical levels), partly to address underresolution of boundary layer processes.

4. Clouds, precipitation and radiation

a. Precipitation

Several precipitation measurements were made at SHEBA. Surface precipitation is difficult to measure accurately in a cold, exposed site, complicating the interpretation of these measurements. The SHEBA Project Office (SPO) maintained a Nipher shielded snow gauge system about 300 m from the SHEBA ship, which was visited daily around 20 UTC. A corrected daily precipitation was computed from the raw value following Goodison and Yang (1996). Corrections are made for wind, losses due to (temperature-dependent) evaporation and gauge wetting, and precipitation amounts in intervals in which the reported weather is blowing (rather than falling) snow are set to

zero. We regard the corrected SPO precipitation time series as the most trustworthy currently available for SHEBA.

The flux tower had both a ETI NOAH-II weighing gauge (which sends a pulse every time it has accumulated 0.254 mm of water equivalent in an antifreeze-containing bucket), and an STI model 815 optical raingauge. The optical raingauge data could not be used for quantitative measurement of water equivalent during the nine months of the SHEBA year when snow was common, and even during rainy periods in the summer season, it indicated 2-3 times as much precipitation as the other raw observation, so we present here only results from the weighing gauge (although in the Appendix we compare radar reflectivities with hourly precipitation time series in which the optical raingauge measurements are used to interpolate between the corrected SPO measurements) . There are a few short gaps in the tower weighing gauge (TWG) data, and one weeklong interval, 19-26 February 1998, during which there are two apparently spurious large precipitation events 'recorded' by the TWG. This was just after a period of ice breakup which required repositioning and recabling of the TWG. Based on a comparison with the SPO precipitation time series, we set the TWG precipitation to zero during both this period and the data gaps. No attempt has been made to correct the TWG results for wind speed, blowing snow, etc., so they should be regarded simply as a qualitative comparison with (and not as trustworthy as) the SPO gauge.

Fig. 7 compares the cumulative precipitation measured by the SPO and TWG with ECMWF. The ECMWF time series is generally similar to the corrected SPO data, with a slight tendency toward less precipitation in the winter and more precipitation in the summer. Fig. 8 compares daily precipitation amounts in July 1998 from the SPO (corrected) and from the ECMWF model, accumulated over 24 hour periods ending at the usual SPO observation time of 20 UTC. Since this is a comparison of a point measurement and a grid-box average, we expect that the SPO (point) measurement will be more intermittent and spiky than the ECMWF prediction, as is seen. However, even with this caveat the agreement is not that good, especially in the summer, when some precipitation events were underforecast (e. g. JD 553-554), and there are several spurious forecasts of precipitation (e. g. JD 556-557 and 563-565) associated with ECMWF-predicted large-scale

midtropospheric upward motion , likely reflecting a poor regional analysis in the model at these times. Hence, a single-column model forced with the ECMWF adiabatic forcing might well be led into similar daily precipitation errors as produced by the ECMWF model itself, regardless of its model physics. For this reason, it is likely more meaningful to compare monthly (or even weekly) statistics of such a single-column model run with observations, rather than comparing daily variations.

b. 8 mm radar observations

The NOAA Environmental Technology Laboratory 35 GHz (8.7 mm wavelength) vertically pointing radar provided an unprecendented view of the variety of Arctic clouds and precipitation throughout the year (Intrieri et al. 2000a). We compared both the occurrence and intensity of radar echoes from cloud and/or precipitation with ECMWF predictions.

For our analysis, we used all available SHEBA profiles (typically one every ten seconds, with 45 m vertical resolution, obtained from the SHEBA data archive) of effective reflectivity Z (mm^6 m^{-3}) and averaged them into hourly profiles. We compared this with a synthetic reflectivity computed from the ECMWF column profiles of cloud liquid and ice water content (q_l and q_i, in kg kg^{-1}) and rain and snow flux (R and S, in mm hr^{-1}). The total synthetic reflectivity is the sum of reflectivities due to cloud water, cloud ice, rain and snow:

$$Z_{EC} = Z_{cw} + Z_{ci} + Z_r + Z_s. \quad (1)$$

Following the approach of B00, the cloud water droplets and ice crystals are assumed to have 6th-power-weighted mean radii of 10 (B00 used 15, but in-situ aircraft data suggest that was an overestimate) and 40 μm; this leads to cloud water/ice reflectivities of

$$Z_{cw} = 50\rho_a q_l \,, \quad (2)$$

$$Z_{ci} = 600\rho_a q_i \,, \quad (3)$$

where ρ_a is the air density in kg m^{-3}.

Synthetic reflectivities associated with rain and snow flux are derived in the Appendix from

curve fits of observed hourly-average reflectivity vs. observed hourly precipitation for the SHEBA year, segregated into rain and snow:

$$Z_r = 7R^{1.32}, \tag{4}$$

$$Z_s = 10S^{0.95}. \tag{5}$$

These relationships were not tuned to the ECMWF model in any way (and in fact, other *Z-R/S* relationships can be found which improve the model/radar agreement).

We summarize some significant points made in the Appendix. Both the *Z-R* and *Z-S* relationships found for SHEBA are different than 'standard' relationships derived previously for midlatitude continental precipitation events sensed by Ka band radars (for which the radar wavelength is short enough so that large hydrometeors are in the Mie, rather than Rayleigh, scattering regime). For Nov. 1997-Jan 1998, and for 15 Apr. 1998 onward, the *Z-S* relationship found is nearly identical to that suggested by B00, and is consistent with a somewhat smaller snowflake size spectrum than in midlatitudes. However, between 1 Feb. - 15 Apr. 1998, there were several snowfalls with hourly-averaged reflectivity of 10-20 dBZ, higher than observed at any other time in SHEBA, yet they did not produce notably large snow accumulations. To prevent massive overestimation of snowfall during this period using (4), we were obliged to cap observed reflectivities at 5 dBZ before using them in a *Z-S* relationship. It is as yet unclear what microphysical characteristics of these snowfalls made them so reflective. Our *Z-R* relationship suggests a raindrop size spectrum dominated by drops about one-half as large for a given rainfall rate than would be predicted by a standard Marshall-Palmer (1948) distribution, but this is hard to reconcile with the observed Doppler fall speeds. Again, it is puzzling why the summertime rain microphysics should be so different than in midlatitudes.

Fig. 9 compares the observed reflectivity with the ECWMF model-synthesized reflectivity for the months of January and July. In general, the timing and vertical extent of radar echo are in qualitative agreement, and clearly are strongly modulated by the passage of extratropical cyclones. These results are similar to Mace et al.'s (1998) findings from an Oklahoma site. However, the

agreement is far from perfect. Tables 2 and 3 test the temporal agreement between measurements and model predictions of the presence of echo exceeding -40 dBZ below and above 2 km over the winter and summer seasons, respectively. During winter, the model is more skilful than in summer. It correctly predicts the echo type 60% of the time (compared to 30% of the time for random guessing). During this season, echo-free periods are fairly common, as are periods of simultaneous echo below and above 2 km. During the summer, when cloud-free conditions are much rarer, the model correctly predicts the echo type 59% of the time vs. 44% by chance alone, and overestimates the frequency of echoes below 2 km.

Fig. 10 shows profiles of the modelled and observed frequency of echoes during the winter and summer seasons, based on three reflectivity thresholds roughly corresponding to detectable cloud, detectable precipitation, and precipitation rates of 2-3 mm day^{-1}, respectively. For all thresholds and in both seasons, the model tends to overestimate the echo frequency, but captures the shape of the profiles. Some overestimation is expected since the ECMWF output is an average over an entire grid cell rather than a point measurement. The ECMWF-predicted cloud fraction (not shown) is only approximately 40-50% of the predicted echo fraction at most heights and in both seasons. While much of this difference simply reflects precipitation falling out of cloud layers, some of it probably also reflects the aggregation of echoes from all clouds in a grid layer into a single area-averaged reflectivity (i. e., even a 20% cloud fraction could lead to a layer-averaged reflectivity exceeding -40 dBZ, and be counted as 100% hourly echo occurrence for that layer. The same accounting is used for the observations, but they represent only an hourly average over a point, which may encompass less cloud variability than an entire grid cell) . The *Z-R* and *Z-S* relationships used, while necessary to make this comparison, also may not capture much of the observed variability in *Z*, even if the precipitation rate were perfectly specified. Despite these caveats, it appears that the model tends to overestimate echo fraction, particularly associated with low clouds in the summertime.

c. Lidar observations of cloud phase

The NOAA vertically pointing Depolarization and Backscatter Unattended Lidar (DABUL) also operated continuously throughout SHEBA, except for February 1998 (Intrieri et al. 2000a). When clouds are present, the linear depolarization ratio δ is an indicator of cloud phase. Nearly spherically symmetrical and optically homogeneous scatterers, such as cloud and drizzle drops, generate near-zero depolarization of the incident energy in the exact backscattering direction, while scatterers with the arbitrary geometry of ice particles, on the other hand, generate values which are typically in the range $\delta \approx 0.4\text{-}\ 0.5$ (Sassen 1991). Typically $\delta<0.1$ is used as a threshold to distinguish clouds with liquid water dominated optical properties(Intrieri et al. 2000a), even though they may contain small concentrations of ice crystals. Intermediate values of δ may indicate mixed-phase clouds. The NOAA group derived and tabulated a δ for each cloud layer detected by the lidar, with a 10 minute sampling frequency. The tabulated δ is a vertical average weighted by the returned power, which we assume mainly comes from near the cloud base (a good assumption except for optically thin clouds).

We selected all 'low' clouds for which the lidar indicated a cloud base below 2 km, and computed the probability density function (PDF) of δ in the winter, spring and summer (Fig. 11). Even in winter, $\delta < 0.1$ for 40% of the times a low cloud was sampled; by summer almost all low clouds have liquid-water dominated optical properties, and the spring case is intermediate. For clouds with bases above 2 km the fraction of liquid-water-dominated clouds decreased significantly (not shown), with $\delta > 0.1$ for more than 80% of the clouds during winter and spring, and 48% during summer.

To assess how depolarization depends on the cloud base temperature we used the rawinsonde soundings that were collected at least twice a day during SHEBA. We assumed that each single temperature profile was representative for three hours before and after its nominal time, and used this to determine cloud base temperature for all lidar data within this time (including both low and other clouds). We binned all data into temperature intervals of 1 K. The fraction of clouds with $\delta < 0.1$ vs. cloud-base temperature, shown in Fig. 12, ramps nearly linearly from 0 at -40 C to 1 at 0

C, suggesting that supercooled droplet clouds were common over SHEBA even at quite low temperatures. Also plotted in Fig. 12 is the average fraction of liquid in the total cloud condensate predicted by the ECMWF parametrization,

$$\alpha = (T - T_{ice})^2/(T_0 - T_{ice})^2, \quad (6)$$

with T the temperature in Kelvin, T_{ice} = 250.16 K and T_0 = 273.16 K. This temperature-dependent partitioning between cloud water and ice ramps quadratically from all ice at and below T_{ice} to all water at T_0. In the model there cannot be liquid water present below T_{ice}, but the lidar indicates that at least 40% of the clouds were mostly in the liquid phase at this temperature. We conclude that the ECMWF parameterization tends to considerably overestimate the proportion of ice in supercooled clouds.

d. Liquid and ice water path

During the SHEBA experiment a microwave radiometer (MWR) was continuously operating at 23.8 and 31.4 GHz to retrieve the vertically integrated water vapor path (WVP) and liquid water paths (LWP) (Liljegren 1994). The 23.8 GHz channel, near the 22.235 GHz water vapor absorption line, is more sensitive to water vapor than cloud liquid water than the 31.4 GHz channel. Both channels are insensitive to ice except under thick precipitating ice cloud layers (Adler et al. 1990). Measurements of the sky radiance at these two frequencies allow the simultaneous determination of the WVP and LWP from a set of two linear equations. Daily mean LWP was computed from the observations. Sometimes the measurements failed due to the presence of water on the window of the instruments. The daily mean was not computed if more than 1/3 of the measurements failed on that day. There is still some controversy about the accuracy of the MWR LWP retrievals, since the most reliable in-situ FIRE-ACE aircraft measurements of LWP over SHEBA (taken in May-Jul. 1998) average only half as large as the simultaneous MWR LWP (J. Curry, 2000, personal communication).

Liquid and ice water path (IWP) were also computed from the ECMWF output. Fig. 13a compares the modelled and observed LWP during March 1998, a typical cold-season month. The EC-

MWF LWP is very small; the model clouds are dominated by ice. However, the MWR data indicate that there was a significant amount of liquid water present during this month, with the observed liquid water paths even exceeding the sum of the ECMWF IWP and LWP. The temperatures in most of the observed cloud layers were generally well above -40 C, so it is plausible that a significant fraction of the clouds consisted of supercooled droplets, in contrast to the ECMWF predictions. Similar results were found for the period January-May 1998. Fig. 13b shows that during June 1998, a typical warm-season month, there is better agreement between the observations and the ECMWF model. The MWR LWP values (which could be computed for all but two days) tend to be systematically somewhat higher than in the model, but similar time variations can be seen in both. There is still considerable ice in the model clouds even in the summer.

e. SurfaceRadiation and Energy Balance

The surface heat budget equation can be expressed as (with upward fluxes positive):

$$LW_{net} + SW_{net} + H + LE = I - M \tag{7}$$

where LW_{net} and SW_{net} represent the net longwave and shortwave radiation, H and LE are the sensible heat and latent heat flux, I the upward conductive energy flux to the top surface of the ice or snow, and M is the heat used to melt ice or snow at the surface. I and M are not computed by the model, so we will treat them as a budget residual. In fact, I and M are an oversimplification of the surface heat transfer, as some solar radiation is absorbed well below the ice surface, and additional heat flux terms are required for leads and melt ponds. One would like to compare the model with an grid-cell area $(60\ \text{km})^2$ averaged surface heat budget, and a continuing objective of SHEBA is to aggregate the many SHEBA observations to construct a best estimate of such a budget. However, for our purposes it suffices to construct a preliminary surface heat budget using flux tower measurements for all budget components except upwelling shortwave radiation. Intrieri et al. (2000b) and Persson et al. (2000) describe these flux tower measurements over the SHEBA annual cycle in much more detail. The downward-pointing pyranometer at the flux tower measured upwelling shortwave radiation from a small area that consisted of a larger percentage of bare ice and

smaller percentage of meltponds during the summer than were present for other areally averaged albedo measurements (Persson et al. 2000). The surface albedo calculated from this measurement was similar to other SHEBA estimates (line-averaged or aerial estimates that averaged across a variety of surface types) in the winter, but up to 15% higher at times in the late summer. Thus, during the melt season (Jun.-Aug.) we computed the upwelling shortwave radiation from the tower-observed downwelling shortwave radiation and an albedo time series linearly interpolated between intermittent measurements along a 300 m line cutting across a variety of surface types (Perovich et al. 1999), which is in reasonable agreement with aircraft estimates (Curry et al. 2000). There are still possible biases in this approach due to unaccounted diurnal variation of albedo, possible bias of Perovich measurements toward clear-sky rather than cloudy conditions, no coverage of leads, etc.; estimation and removal of such biases in upwelling shortwave radiation (which could be as much as 10 W m^{-2} in a monthly mean) constitutes a major challenge for SHEBA. These biases are probably at least as large as the standard errors of the tower-measured monthly radiation components, which we estimate to be less than 5 W m^{-2}. In general, our heat budget underestimates or effectively ignores leads, which again may bias our estimates of some monthly-average heat flux components by a few W m^{-2}.

Due to instrumentation problems, or to the removal of turbulence flux data when the airflow was from the ship, some observations were discarded. In particular, the majority of the observed eddy correlation latent heat flux observations is considered unreliable, so except for Aug.-Sep. 1998 we instead used the SHEBA Atmospheric Surface Flux Group bulk-aerodynamic estimates of *LE (*also obtained from the SHEBA data archive). Over the entire SHEBA year,79% of the turbulent heat flux data and at least 90% of the radiation data were usable. The monthly standard error in turbulent heat flux is estimated to be 2 W m^{-2}.

The ice heat flux *I,* deduced from ice temperature profiles, ranges from slightly over 10 W m^{-2} in midwinter months to near zero in the summer. The ice surface group estimated the ice melt rate along the same line used to calculate albedo; converting this into a latent heat of melting implies *M* is as large as 60 W m^{-2} in June and July (Perovich et al. 1999). These estimates are broadly con-

sistent with the residual I - M deduced from the surface observations. However, at this time we do not have sufficiently reliable monthly averaged, areally aggregated estimates of I and M to use as a check on the budget residual estimates of I - M presented in Table 4. To get a sense of the accuracy with which one would like to know I-M, an annually averaged I - M of -10 W m^{-2} would correspond to the surface melting of approximately 1 m of ice over the year.

Table 4 compares monthly-mean values of the heat budget components from the model results and the SHEBA observations. The ECMWF model overestimates LW_{net} by about 30 W m^{-2} between November 1997 and May 1998, due to reinforcing systematic errors in the upward and downward components. Fig. 14 shows daily observed (from the SHEBA flux tower) and modelled downwelling longwave radiation for the winter and summer seasons. During clear periods and during summer, the downwelling longwave radiation is fairly accurately estimated. During some cloudy winter and spring periods (e.g. Julian days 372-376 and 391-395), the daily average modelled downwelling longwave radiation is up to 50 W m^{-2} lower than observed. In the previous section, we noted that the model clouds predicted in this period consist mainly of ice, when lidar observations suggest that water cloud layers are common. Since ice particles typically have a much larger size than liquid water droplets, the cloud optical depth and albedo of an ice cloud will be lower than those of a liquid water cloud with the same total cloud water content. In the radiation parameterization used in the ECMWF model, the assumed cloud droplet effective radius (r_e) for ice clouds ranged from 40 μm at very cold temperatures to 130 at temperatures exceeding 250 K (Ou and Liou, 1995); for liquid water cloud r_e was parameterized as a linear function of height from 10 μm near the surface (where most water cloud in the model is) to 45 μm at the top of the atmosphere. We hypothesize that this, combined with the bias toward ice cloud, leads to wintertime clouds in the model that are optically too thin and insufficiently emissive. The upwelling longwave radiation tends to be erroneously large owing to a wintertime ice surface temperature that is on average too high.

The model overestimates the downwelling shortwave radiation at the surface in nearly all months. This is again consistent with underestimation of cloud optical depth. It is less clear why

the model overpredicts the downward shortwave radiation for the summer months July and August since the low cloud fraction is overestimated by the model, and its LWP is in a better agreement with the MWR observations - one small contributor could be multiple scattering between the model's ice surface (which is overly reflective in these months) and the low clouds.

The monthly-mean albedos in Table 4 vary from 0.85 before the melt season to 0.47 in mid-summer. The albedo in the ECMWF model has a constant value of 0.59. This also contributes to large biases in upwelling and net shortwave radiation in the model. The effect of the model albedo bias is clear from looking at the upwelling shortwave radiation in May vs. July. In May, the ECMWF-assumed albedo is too low and upwelling shortwave radiation is underestimated by 40 W m^{-2}; the reverse is true by July. Thus the largest monthly bias in net shortwave radiation, -70 W m^{-2}, occurs in May, when upwelling shortwave radiation is underestimated but downwelling shortwave radiation is overestimated, while the bias reverses later in the summer.

The observed monthly-averaged turbulent heat flux is small over the entire SHEBA year. The model predicts a mean downward turbulent heat flux for all months, and averaged over the whole SHEBA period the modeled turbulent heat flux is about 4.6 W m^{-2} less than the observations. The latent heat flux is small in both models and measurements in the winter; in the summer the ECMWF latent heat flux is approximately twice as large as the bulk estimates from the flux tower, a systematic error of up to 4 W m^{-2}.

The biases of the modeled net longwave and shortwave radiation are reflected in the model error in the residual term, $(I\text{-}M)_{EC} - (I\text{-}M)_{obs}$, which is up to 30 W m^{-2} in the winter months and as low as -37 W m^{-2} in May, before turning weakly positive again in the summer months. Averaged over the whole SHEBA year, the model residual is 10 W m^{-2} larger than the observations; a 20 W m^{-2} excess in LW_{net} is partly balanced by a 10 W m^{-2} underestimation of SW_{net}.

5. Conclusions

We have compared the ECMWF model with an integrated suite of data over the annual cycle at the SHEBA ice station. The atmospheric dynamics and the associated cloud distribution in the

SHEBA column were quite complex and synoptically variable during all parts of the annual cycle. In general, the ECMWF model appears to have faithfully captured the time variations of pressure, temperature, and to a lesser extent, humidity over the SHEBA column. At the same time, it maintained a close balance between the adiabatic and diabatic tendencies of temperature and moisture, a sign that the model was not systematically drifting away from the observed soundings of temperature and humidity. It also predicted precipitation fairly skilfully averaged over weekly and longer timescales (though not so well on daily timescales), which lends credibility to the model vertical motion profiles. Together, these suggest that the model-predicted adiabatic tendencies are probably satisfactory for forcing single-column models.

The ECMWF model did a reasonable job of predicting the timing and vertical distribution of cloud. However, the SHEBA measurements allowed the diagnosis of some problems in the model cloud, boundary layer, and surface physics. In winter, the isothermal slab ice model heavily damped the surface air temperature variability, and the model frequently predicted spurious large downward turbulent heat flux, as noted by B00. We suggest that the latter problem may partly be due to vertical under-resolution of the dynamics of stable shear-driven boundary layers under strong-wind conditions. The model considerably overestimated the ice fraction in supercooled clouds, and biases in downwelling shortwave and longwave radiation suggest that the modelled optical depth of these clouds was too low, perhaps due to substitution of large ice crystals for small water droplets. The fixed albedo and poor skin temperature in the model led to further errors in the net radiative fluxes. As a result of our study, ECMWF will soon introduce a new four-layer sea-ice model with prescribed seasonal variability of albedo (P. Viterbo, personal communication, 2000).

Acknowledgments

We wish to thank the many SHEBA investigators who helped gather the data in this study, most notably our colleagues in the SHEBA Atmospheric Surface Flux Group, Chris Fairall, Peter Guest, and Ola Persson for help collecting and processing the surface meteorology, turbulence, and radiation data. Taneil Uttal of the NOAA/ETL remote sensing group provided the radar data, and, with

Sergei Matrosov, was very helpful in interpreting it. Matt Shupe of NOAA/ETL helped to process the lidar data. The microwave radiometer data were collected and provided by Dr. J. Liljegren (Iowa State University). Sarah Dreckman, sponsored by the NASA Space Grant Program for summer research by undergraduates, helped download and analyze some of the data. We thank Drs. A. Beljaars and P. Viterbo of ECMWF for their very constructive comments on early versions of this manuscript. Drs. Bretherton and De Roode were supported by NASA grant NAG1-2072. The National Science Foundation supported Dr. Andreas and the ASFG research with grants to the U.S. Army Cold Regions Research and Engineering Laboratory, NOAA's Environmental Technology Laboratory, and the Naval Postgraduate School, and supported Dr. Moritz and the SHEBA Project Office through grant NSF-OPP9720144.

Appendix. Empirical Z-R and Z-S relationships for SHEBA

Our goal is to distinguish between characteristic reflectivities associated with heavy, light, and no precipitation, falling as either rain or snow, to allow ECMWF-synthesized and observed radar reflectivities to be broadly compared. This does not require highly accurate *Z-R* and *Z-S* relationships. This is fortunate, as such relationships derived from the in-situ SHEBA observations show a lot of scatter, are substantially different from previously-derived midlatitude continental *Z-R* and *Z-S* relationships, and raise interesting questions about the SHEBA cloud microphysics.

Hourly precipitation was estimated from the corrected SPO time series. This quasi-daily time series was converted to an hourly time series by rescaling the hourly precipitation accumulations estimated by the flux tower optical rain gauge to match the SPO time series. While the best we can currently do, this procedure may be quite inaccurate, especially in light snowfall.

Hourly reflectivity at 0.4 km was compared with surface precipitation, as reflectivities at levels closer to the ground sometimes appeared to be anomalously low. The data were segregated into 'rain' periods where the ECMWF-analyzed level-29 (500 m) temperature exceeded 273 K or the radar-derived mean Doppler fall speed exceeded 3 m s^{-1}; other periods were categorized as 'snow'.

Fig. 15a plots *Z* vs. *R* for the rain periods. There is considerable scatter, but some correlation. Wexler and Atlas (1963) computed that for a standard Marshall-Palmer exponential distribution of raindrop diameters and a Ka-band radar,

$$Z_r = 350\, R^{1.32} \text{ for rainfall rates } R < 5 \text{ mm hr}^{-1} \qquad \text{(A1)}$$

which suffices for rain events observed at the SHEBA ship. This line, dashed in Fig. 15a, is clearly an overestimate of *Z* given *R*. Since the dominant precipitation events had $R \sim 1$ mm hr^{-1}, tuning the exponent would have little effect, so we tuned only the constant. Our fit (4), in which 350 is replaced by 7, is shown as the dot-dashed line in Fig. 15a. This *Z-R* relation fairly accurately predicts the cumulative summertime (Jun-Aug) precipitation at SHEBA, most of which fell as rain, from the observed hourly-averaged reflectivity (Fig. 16). By comparison, the standard *Z-R* relation underpredicts cumulative summer precipitation by a factor of 50! This enormous discrepancy sug-

gests that the drops dominating the reflectivity must be much smaller than predicted by the standard Marshall-Palmer drop spectrum. However, the Doppler fall speeds of 5-6 m s^{-1} typically observed during more intense rain are not compatible with such small drops. Further study of this issue is required.

Matrosov (1992) related Ka-band reflectivity to snowfall rate S (mm hr^{-1} water equivalent) following methodology of Sekhon and Srivastava (1970). His relationship is senstive to the assumed density of the falling snow crystals, which is unknown; for ρ_s = 0.06 g cm^{-3} it is

$$Z_s = 28S^{0.95}. \qquad \text{(A2)}$$

Fig. 15b plots Z_s vs. S for the snow periods. One puzzling feature of this plot is that the strongest reflectivities in snow, between 10-20 dBZ, seem almost totally uncorrelated with surface accumulation rate! All of these events occur between 1 Feb-15 Apr 1998. Fig. 16 shows that if Matrosov's formula is used, these high-reflectivity events excessively dominate the wintertime snow accumulation. At other times, reflectivity rarely exceeds 5 dBZ, but again there is rather little correlation between reflectivity and snow accumulation rate. Nevertheless, as long as reflectivities are capped at 5 dBZ, (5), shown as the dashed line in Fig. 15b, gives a reasonable fit to the month-by-month accumulated precipitation over SHEBA (Fig. 16). This truncation prevents the high-reflectivity snow events (all of which do correspond to Doppler fall speeds of approximately 1 m s^{-1}, so do seem to really correspond to falling crystals) from unrealistically dominating the reflectivity, but since it has no physical basis, more investigation is clearly warranted.

References

Adler, R. F., R. A. Mack, N. Prasad, I. M. Hakkarinen, H.-Y. M. Yeh, 1990: Aircraft microwave observations and simulations of deep convection from 18 to 183 GHz. Part I: Observations. *J. Atmos. Oceanic Technol*., **7**, 377-391.

Andreas, E.L., C.W. Fairall, P.S. Guest, and P.O.G. Persson, 1999: An overview of the SHEBA atmospheric surface flux program. Fifth Conference on Polar Meteorology and Oceanography of the American Meteorological Society, 411-416.

Beesley, T. A., C. S. Bretherton, C. Jakob, E. L Andreas, J. M. Intrieri, and T. A. Uttal, 2000: A comparison of the ECMWF forecast model with observations at SHEBA, *J. Geophys. Res.* , in press.

Curry, J. A., and 26 coauthors, 2000: FIRE Arctic clouds experiment. *Bull. Amer. Meteor. Soc.*, **81**, 5-29.

Goodison, B.E. and D. Yang, 1996: In-situ measurement of solid precipitation in high latitudes: the need for correction. *Proc. of the Workshop on the ACSYS Solid Precipitation Climatology Project*, Reston, VA, USA, 12-15 Sept. 1995, WCRP-93, WMO/TD No. 739, pp. 3-17.

Intrieri, J. M., M. D. Shupe, B. J. McCarty, and T. Uttal, 2000a: Annual cycle of arctic cloud statistics from lidar and radar at SHEBA. *J. Geophys. Res.*, submitted 5/00.

Intrieri, J. M. , C. W. Fairall, M. D. Shupe, P. O. G. Persson , E. L Andreas, P. S. Guest , and R. E. Moritz, 2000b: Annual Cycle of Arctic Cloud Forcing at SHEBA. *J. Geophys. Res*., submitted 5/00.

Liljegren, J. C., 1994: Two-channel microwave radiometer for observations of total column precipitable water vapor and cloud liquid water path. *Proc. Fifth Symp. on Global Change Studies*, Nashville, TN, Amer. Meteor. Soc., 262-269.

Mace, G. G., C. Jakob, and K. P. Moran, 1998: Validation of hydrometeor prediction from the ECMWF model during winter season 1997 using millimeter wave radar data. *Geophys. Res. Lett.*, **25**, 1645-1648.

Marshall, J. S., and Palmer W. McK.., 1948: The distribution of raindrops with size. *J. Meteor.*,

5, 165-166.

Matrosov, S. Y., 1992: Radar reflectivity in snowfall. *IEEE Trans. Geosci. Remote Sensing.* **30**, 454-461.

Miller, S. D., G. L. Stephens, and A. C. M. Beljaars, 1999: A validation survey of the ECMWF prognostic cloud scheme using LITE. *Geophys. Res. Lett.*, **26**, 1417-1420.

Ou, S., and K.-N. Liou, 1995: Ice Microphysics and Climatic Temperature Feedback, *Atm. Res*., 35, 127-138.

Perovich, D. K., T. C. Grenfell, B. Light, J. A. Richter-Menge, M. Sturm, W. B. Tucker III, H. Eicken, G. A. Maykut, and B. Elder, 1999: *SHEBA: Snow and Ice Studies CD-ROM*. Obtainable from D. Perovich, CRREL, 72 Lyme Road, Hanover, NH, USA 03755.

Persson, P. O. G, C. W. Fairall, E. L. Andreas, and P. S. Guest, 2000: Measurements of the Meteorological Conditions and Surface Energy Budget Near the Atmospheric Surface Flux Group Tower at SHEBA, *J. Geophys. Res.*, submitted.

Sassen, K., 1991: The polarization lidar technique for cloud research: A review and current assessment. *Bull. Amer. Meteor. Soc.*, **72**, 1848-1866.

Sekhon, R. S., and R. C. Srivastava, 1970: Snow size spectra and radar reflectivity. *J. Atmos. Sci.*, **27**, 299-307

Viterbo, P., A. Beljaars, J.-F. Mahfouf, and J. Teixeira, 1999: The representation of soil moisture freezing and its impact on the stable boundary layer. *Quart. J. Roy. Met. Soc.*, 125, 2401-2426.

Wexler, R., and D. Atlas, 1963: Radar reflectivity and attenuation of rain. *J. Appl. Meteor.*, **2**, 276-280.

Table 1: Data sources. ASFG denotes the SHEBA Atmospheric Surface Flux Group, SPO the Sheba Project Office, and NOAA/ETL is the National Oceanic and Atmospheric Administration Environmental Technology Laboratory

Parameter	Instrument	Investigator	Frequency
Surface air pressure	Vaisala PTB 220B	ASFG	1 hr
2.5 m temperature 10 m vector wind	Vaisala HMP235 ATI sonic anemometer.	ASFG	1 hr average
Temp., humidity profiles	Vaisala GPS sondes	SPO	12 hr
Turbulent heat flux	ATI sonic anemometer	ASFG	1 hr average
Reflectivity	35 GHz Doppler radar	NOAA/ETL	10 min.
Cloud base, depolarization	523 nm DABUL lidar	NOAA/ETL	10 s
Liquid water path	Microwave radiometer	Liljegren	1 hr average
Down/up welling longwave	Eppley pyrgeometer	ASFG	1 hr average
Down/upwelling shortwave	Eppley pyranometer	ASFG	1 hr average
Line-averaged albedo	Kipp & Zonen albedometer	Perovich	Irregular
Precipitation	Nipher shielded snow gauge	SPO	~ daily
Precipitation	ETI weighing gauge Optical rain gauge	ASFG	1 hr
Model ‘analyses’ (12-35 hr forecasts)	ECMWF forecast model, cycle CY18R6 (T_L319 L31 resolution)	ECMWF	1 hr average

Table 2: Joint distribution (%) of hourly observed and ECMWF echo type, Jan.-Mar. 1998

ECMWF\Obs	No echo	< 2 km	>2 km	Both	Total
No echo	26	4	3	1	34
< 2 km only	11	5	1	4	22
>2 km only	2	0.3	4	2	9
Both layers	3	5	1	25	34
Total	43	16	10	32	100

Table 3: Joint distribution (%) of hourly observed and ECMWF echo type, Jun.-Aug. 1998

ECMWF\Obs	No echo	< 2 km	>2 km	Both	Total
No echo	0.3	0.5	0.1	0.6	1
< 2 km only	6	12	3	12	32
>2 km only	0.3	0.1	1	1	3
Both layers	5	7	7	46	64
Total	11	19	11	59	100

Table 4: The observed and ECMWF model predicted net shortwave and longwave radiation, and the sensible heat flux in W m^{-2} (upward is positive). The error in the net radiation is computed as $\Delta X_{net} = (X_{up,EC} - X_{dn,EC}) - (X_{up,obs} - X_{dn,obs})$, with X either *SW* or *LW*.

	Nov	Dec	Jan	Feb	Mar	Apr	May	Jun	Jul	Aug	Sep	All
$LW_{dn,obs}$	209.8	152.0	171.9	155.5	205.1	219.0	245.8	282.3	299.5	299.4	284.1	231.9
$LW_{up,obs}$	227.3	185.2	197.2	188.3	221.3	242.1	273.7	309.0	314.5	310.7	295.6	252.3
$LW_{dn,EC}$	188.1	144.6	152.5	148.8	176.1	194.5	233.9	282.4	296.8	296.3	276.5	217.5
$LW_{up,EC}$	239.7	206.6	199.9	204.2	222.5	254.7	292.1	307.2	307.5	307.4	298.6	258.5
ΔLW_{net}	34.2	28.8	22.2	22.6	30.2	37.1	30.3	-1.9	-4.2	-0.2	10.5	20.6
$SW_{dn,obs}$	0.0	0.0	0.0	5.1	42.8	141.6	248.6	282.2	207.2	111.8	41.6	101.3
$SW_{up,obs}$	0.0	0.0	0.0	4.2	35.6	117.4	205.3	175.9	99.1	55.8	30.2	67.7
$SW_{dn,EC}$	0.0	0.0	0.0	3.2	47.0	151.7	273.3	294.1	226.2	128.4	43.4	107.0
$SW_{up,EC}$	0.0	0.0	0.0	1.9	27.8	89.8	161.8	174.1	133.9	76.0	25.7	63.3
ΔSW_{net}	0.0	0.0	0.0	-0.4	-12.0	-37.7	-68.2	-13.7	15.9	3.6	-6.3	-10.1
Albedo	-	-	-	0.85	0.85	0.86	0.85	0.63	0.47	0.50	0.74	0.68
H_{obs}	-2.6	-5.7	-5.4	-8.0	-2.9	-0.6	1.6	0.3	-2.6	2.4	0.1	-1.9
H_{EC}	-6.3	-6.0	-14.4	-12.5	-8.6	-4.3	-4.4	-3.3	-6.0	-5.0	-0.1	-6.5
LE_{obs}	0.7	-0.1	0.2	-0.1	0.4	0.5	4.2	5.1	-0.1	2.2	1.4	1.1
LE_{EC}	0.6	1.0	-0.1	0.6	1.2	4.2	9.4	6.8	3.8	4.4	7.1	3.6
$(I\text{-}M)_{obs}$	15.6	27.4	20.1	23.9	6.6	-1.1	-9.7	-74.1	-96.0	-40.1	1.7	-14.0
$(I\text{-}M)_{EC}$	46.0	57.0	33.0	42.1	19.7	-1.5	-46.9	-88.8	-80.8	-40.6	11.6	-4.7

List of Figures

ly liquid cloud layer) and the parameterized liquid fraction of the cloud condensate in the ECMWF model as functions of rawinsonde-derived cloud-base temperature.

Figure 13. Daily-averaged liquid water path from the MWR and from ECMWF, and IWP from ECMWF, for (a) Mar. 1998, and (b) Jun. 1998.

Figure 14. Observed and model-predicted downwelling surface longwave radiation.

Figure 15. Observed hourly-average reflectivity at 400 m vs. precipitation rate for (a) rain (T > 273 K or mean fall speed > 3 m s^{-1}) and (b) snow (all other times).

Figure 16. Cumulative precipitation from corrected SPO measurements compared with predictions based on from hourly-average reflectivity at 400 m and two *Z-R/S* relations - our empirical relations (4-5) (using a 5 dBZ reflectivity cap for snowfall) and the standard midlatitude relations (A1-A2).

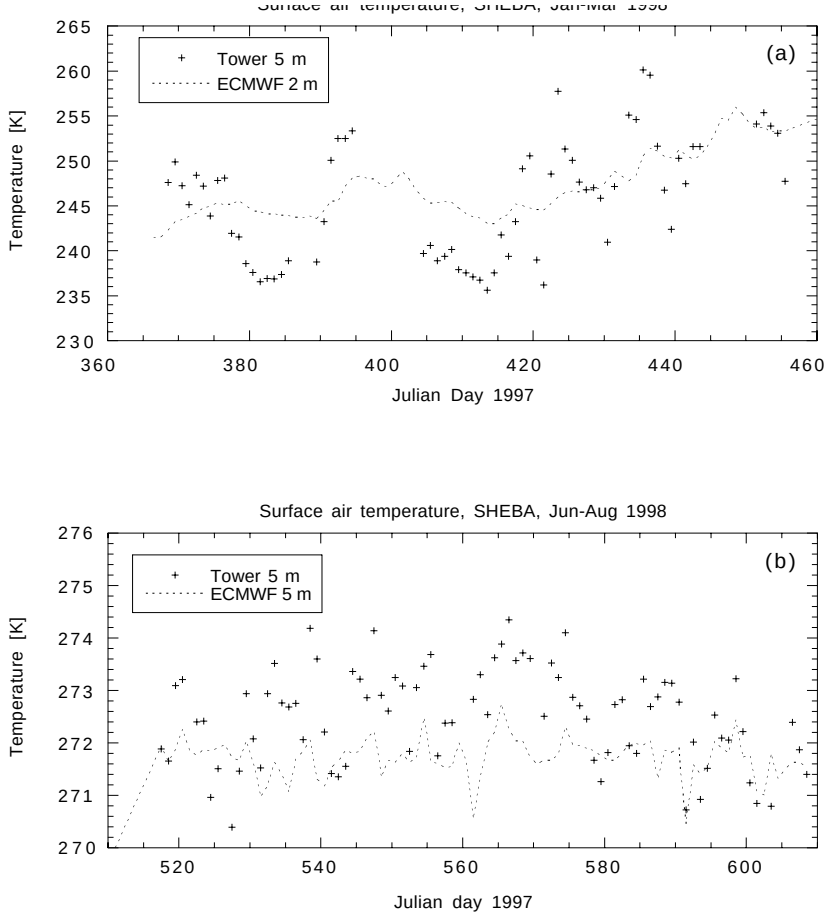

Figure 1. Daily average air temperature measured interpolated to 2.5 m from the SHEBA flux tower, and ECMWF 2 m air temperature for (a) Jan.-Mar. 1998, and (b) Jun.-Aug. 1998. During Aug. 1998, plotted temperatures are from the lowest flux-tower temperature sensor, which was slightly more than 2.5 m above the ice at this time due to summer ice melt.

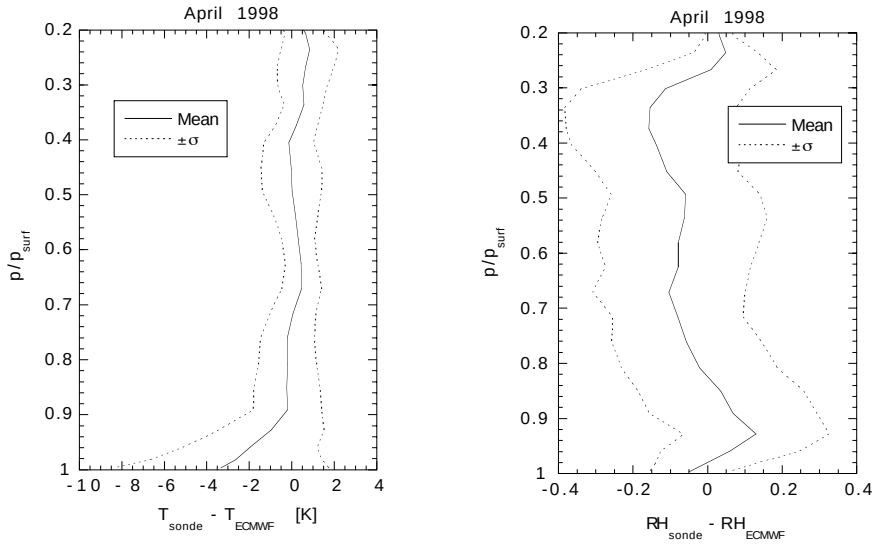

Figure 2. Distribution of difference of ECMWF and rawinsonde temperature and relative humidity (sampled twice daily) for April 1998. Solid lines are the vertical profiles of monthly mean EC-MWF bias, and dashed lines indicate one standard deviation of the instanteous bias from from its monthly mean.

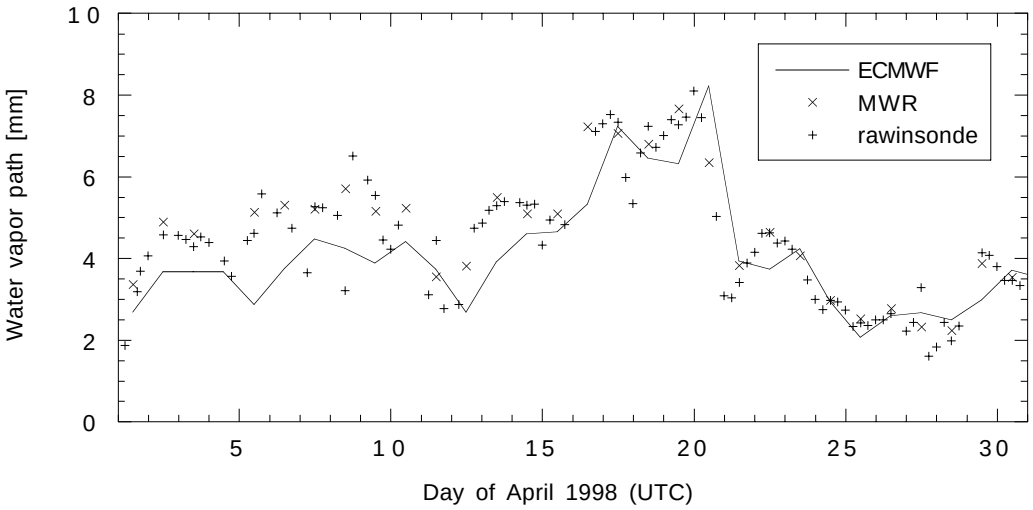

Figure 3. SHEBA column water vapor path for April 1997 from ECMWF analysis, sonde ascents, and microwave radiometer retrievals.

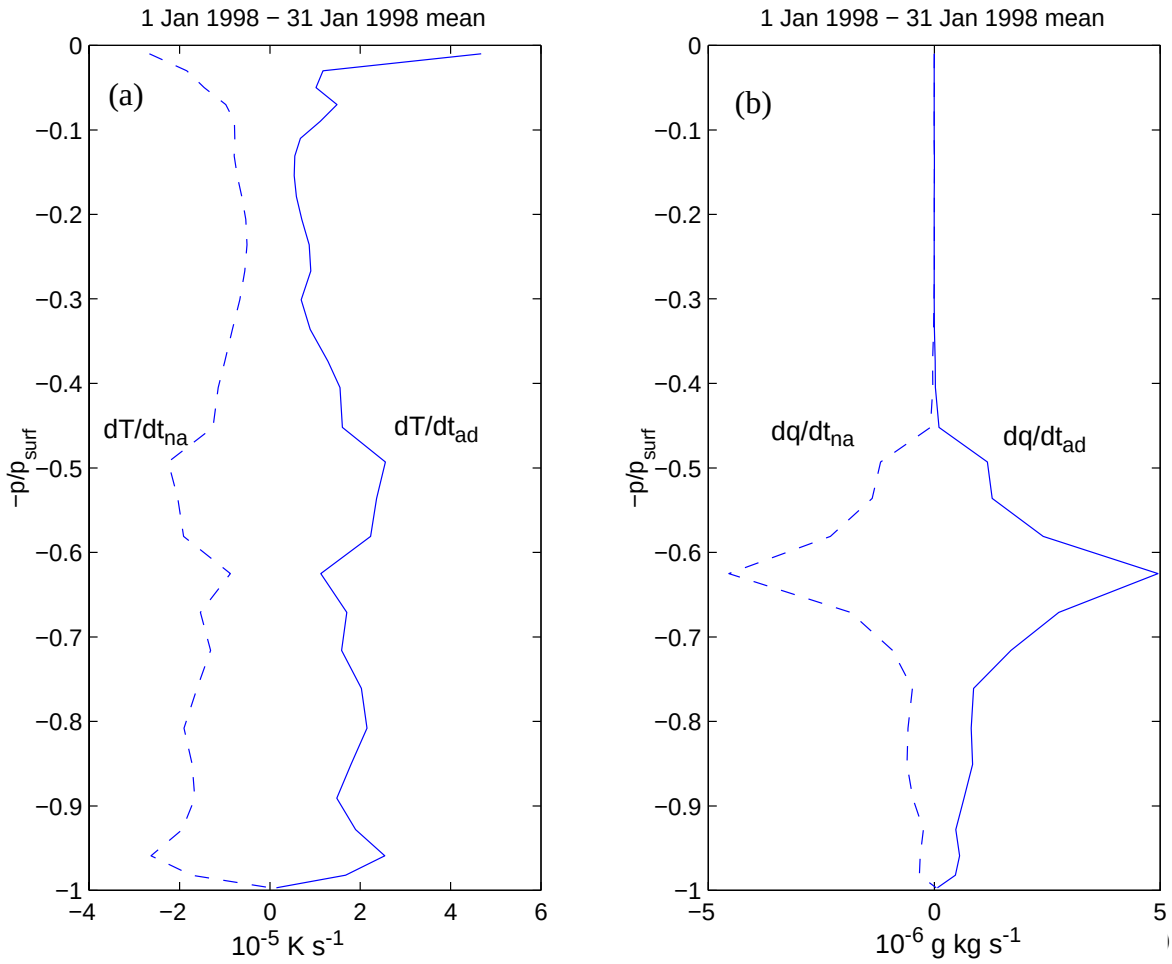

Figure 4. ECMWF adiabatic and nonadiabatic tendencies for Jan. 1998 of (a) heat and (b) moisture.

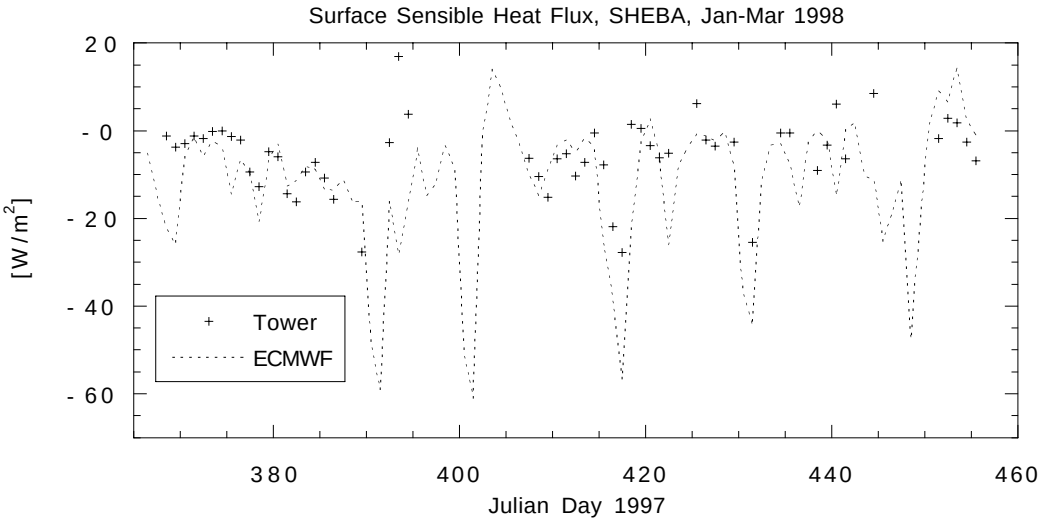

Figure 5. Daily-averaged surface sensible heat flux measured on the SHEBA flux tower and predicted by ECMWF for Jan.-Mar. 1998.

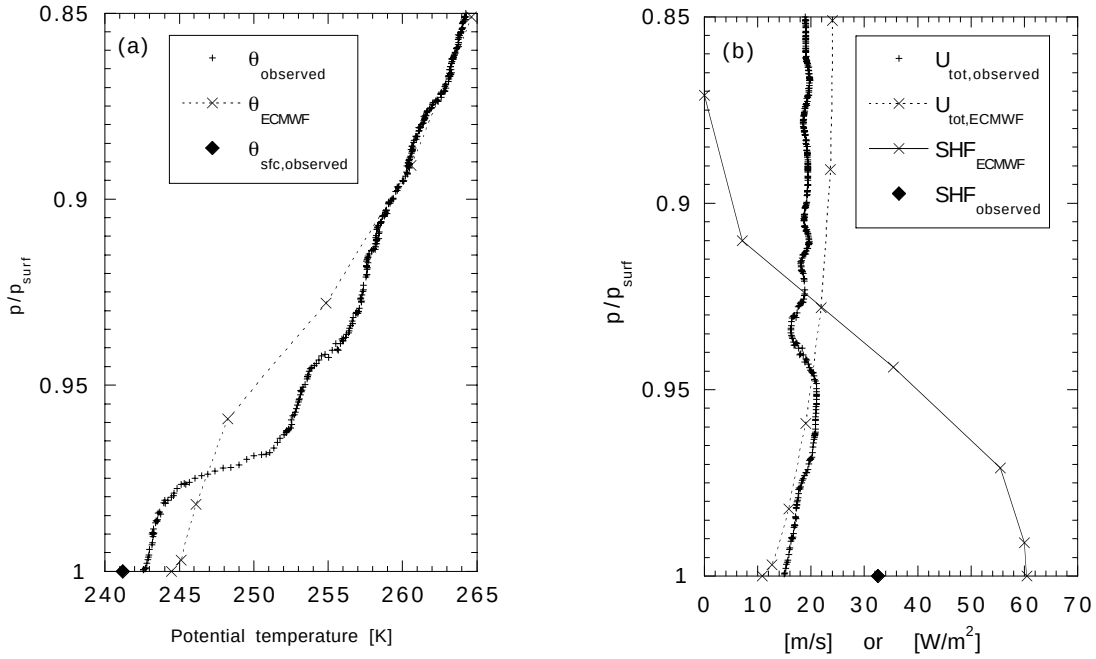

Figure 6. Profiles from 11:15 UTC 21 Feb. 1998 of: (a) Model and observed potential temperature, and (b) model and observed winds and model downward turbulent heat fluxes (the diamond marks the observed downward surface sensible heat flux).

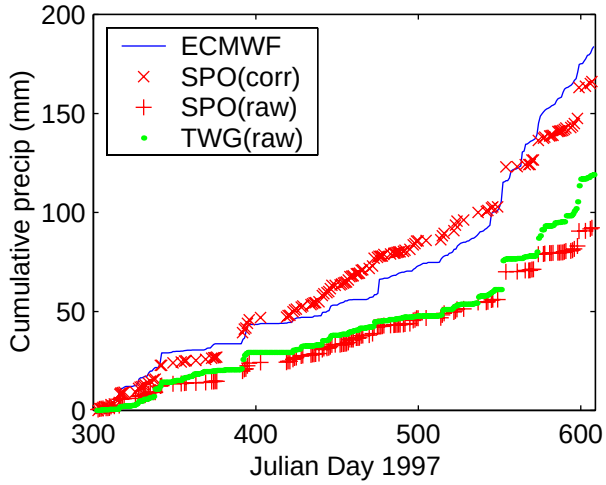

Figure 7. Cumulative precipitation at SHEBA starting on 29 Oct.1997 (Julian Day 302) from EC-MWF, the SPO gauge (corrected and uncorrected), and the tower weighing gauge (TWG).

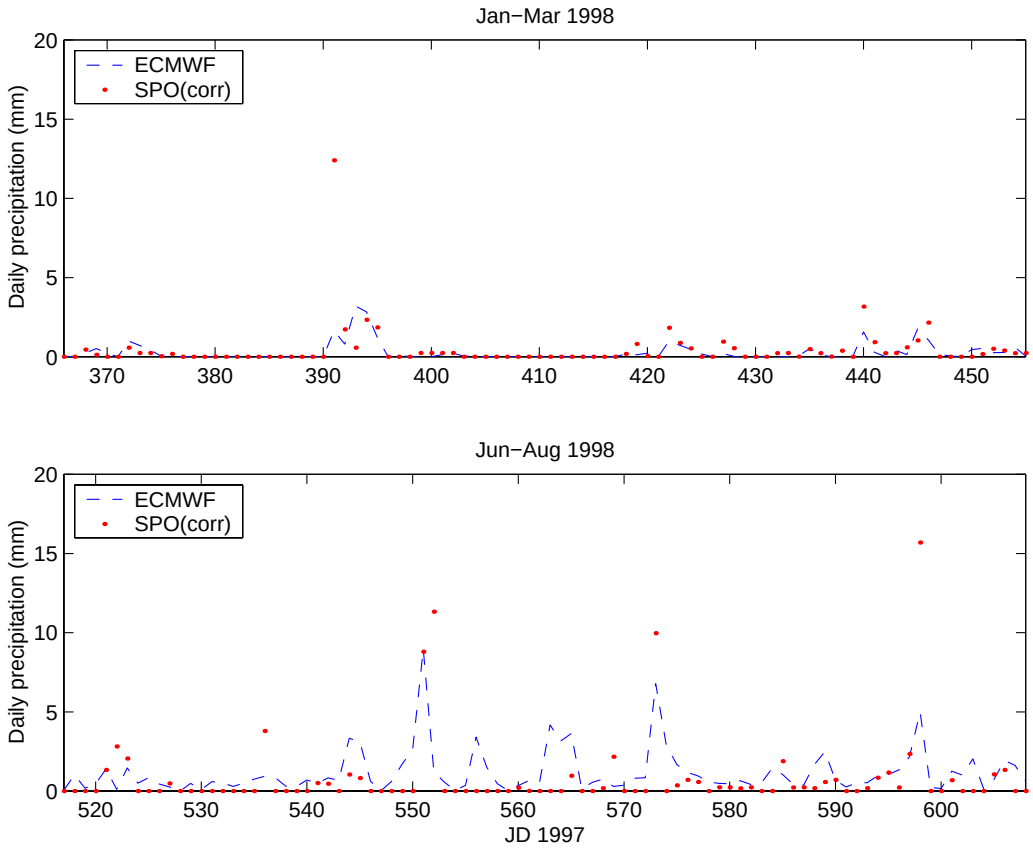

Figure 8. SPO corrected precipitation and model-predicted precipitation for 24 hour periods ending at 20 UTC each day (to match the usual observation time).

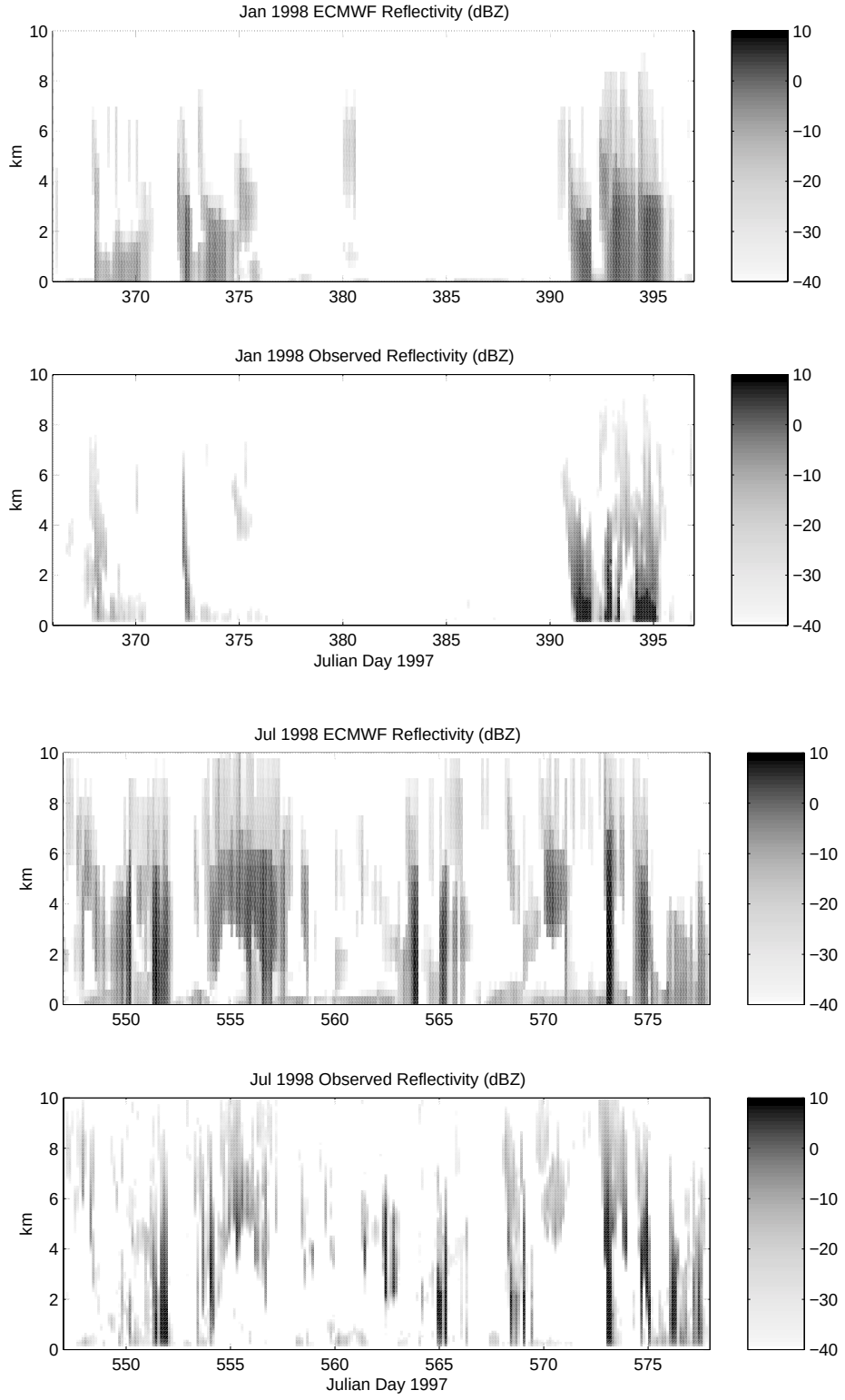

Figure 9. ECMWF-synthesized and observed radar reflectivities for Jan. and Jul. 1998.

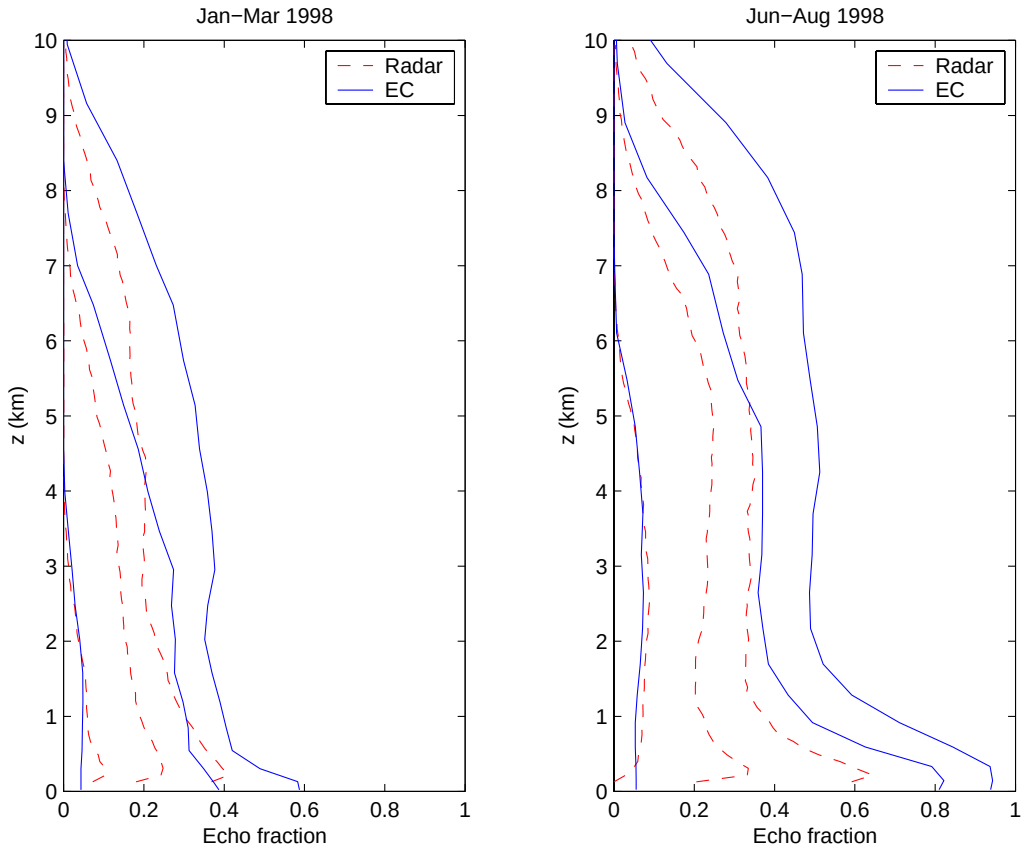

Figure 10. Winter and summer mean profiles of the fraction of time ECMWF-synthesized and radar-observed reflectivities exceeded 0 (left curves), - 20 (middle curves), and -40 dBZ (right curves).

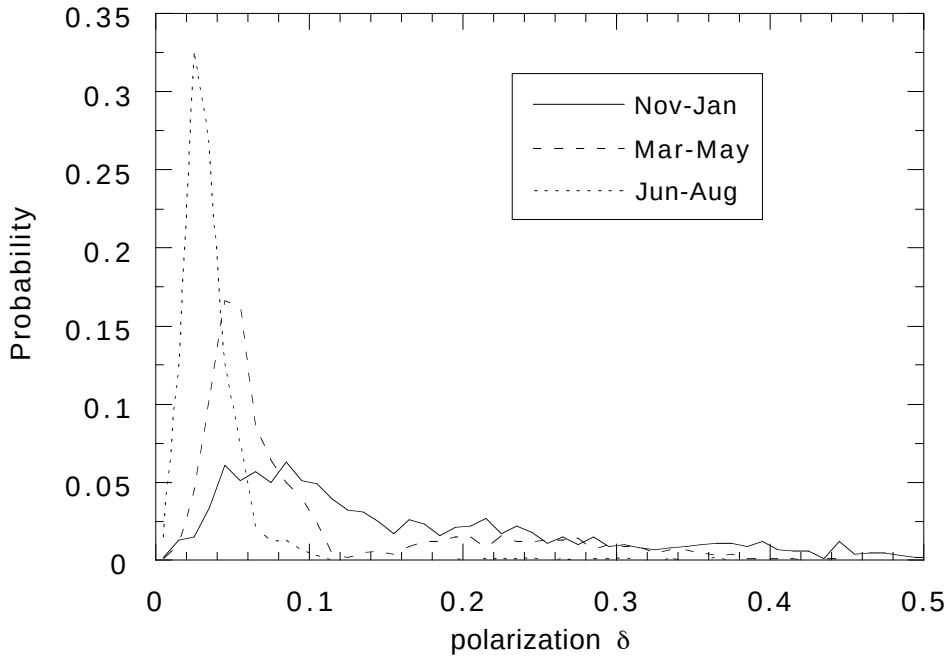

Figure 11. The probability density function of the polarization for three selected periods for all clouds below 2 km.

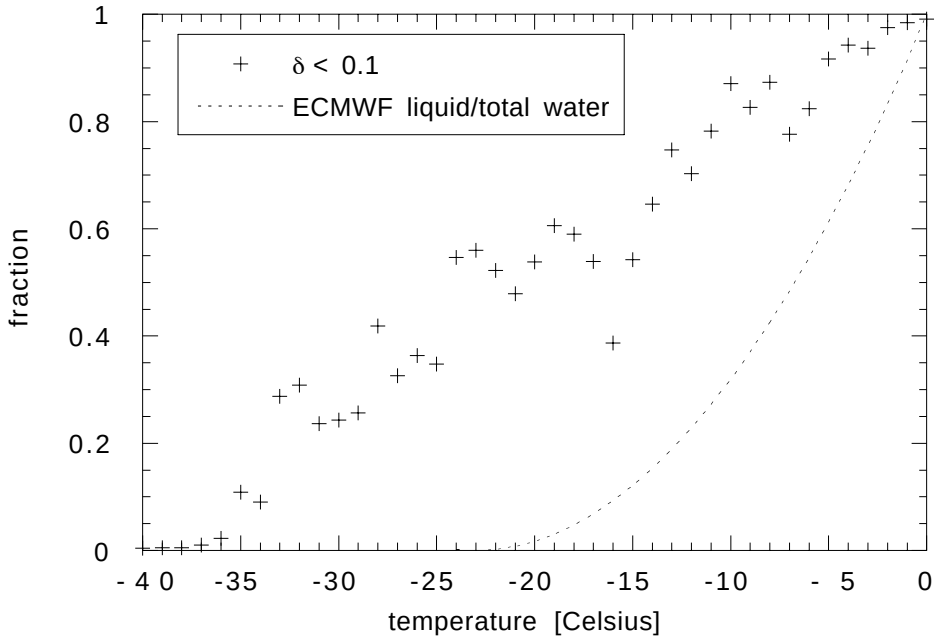

Figure 12: The fraction of cloud layers with lidar depolarization $\delta < 0.1$ (indicating a predominantly liquid cloud layer) and the parameterized liquid fraction of the cloud condensate in the ECMWF model as functions of rawinsonde-derived cloud-base temperature.

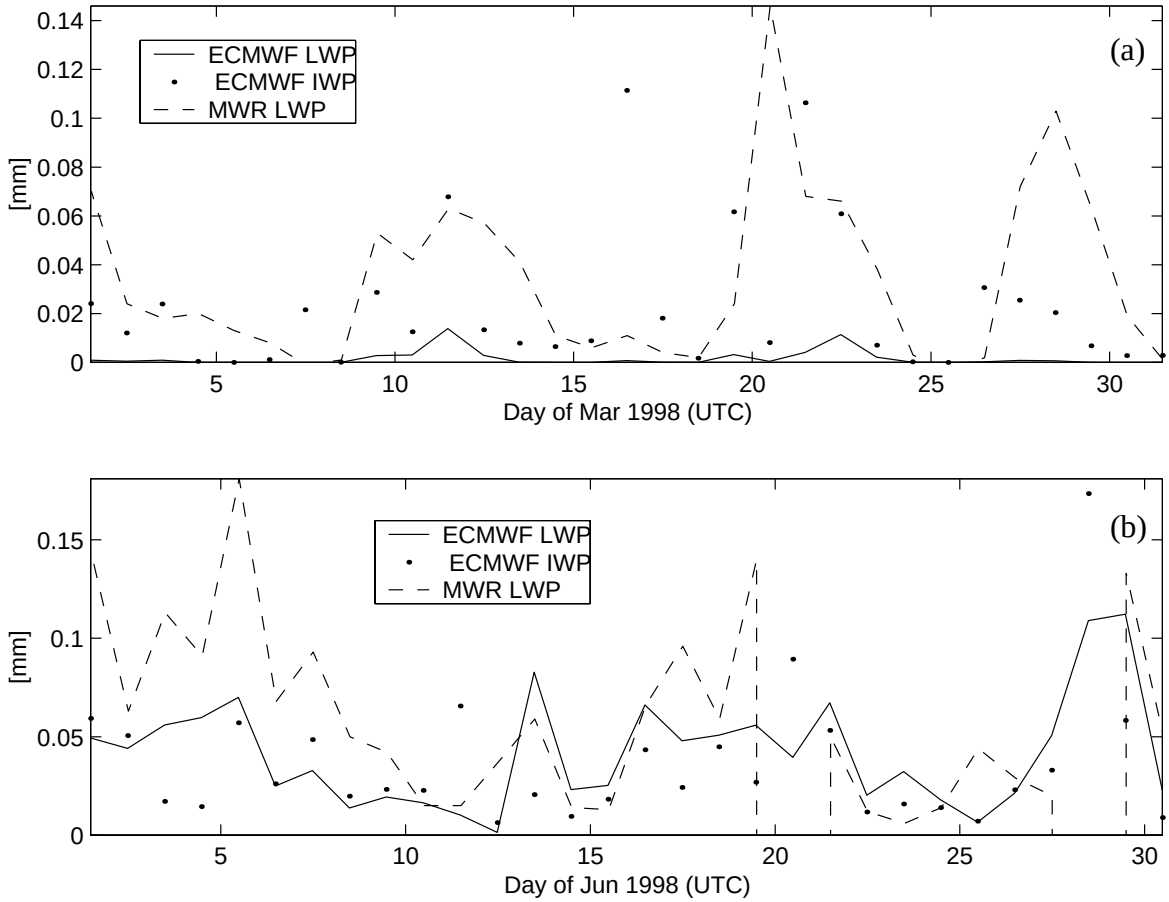

Figure 13. Daily-averaged liquid water path from the MWR and from ECMWF, and ice water path from ECMWF, for (a) March 1998, and (b) June 1998. MWR data was not available around 20-21 and 28 June.

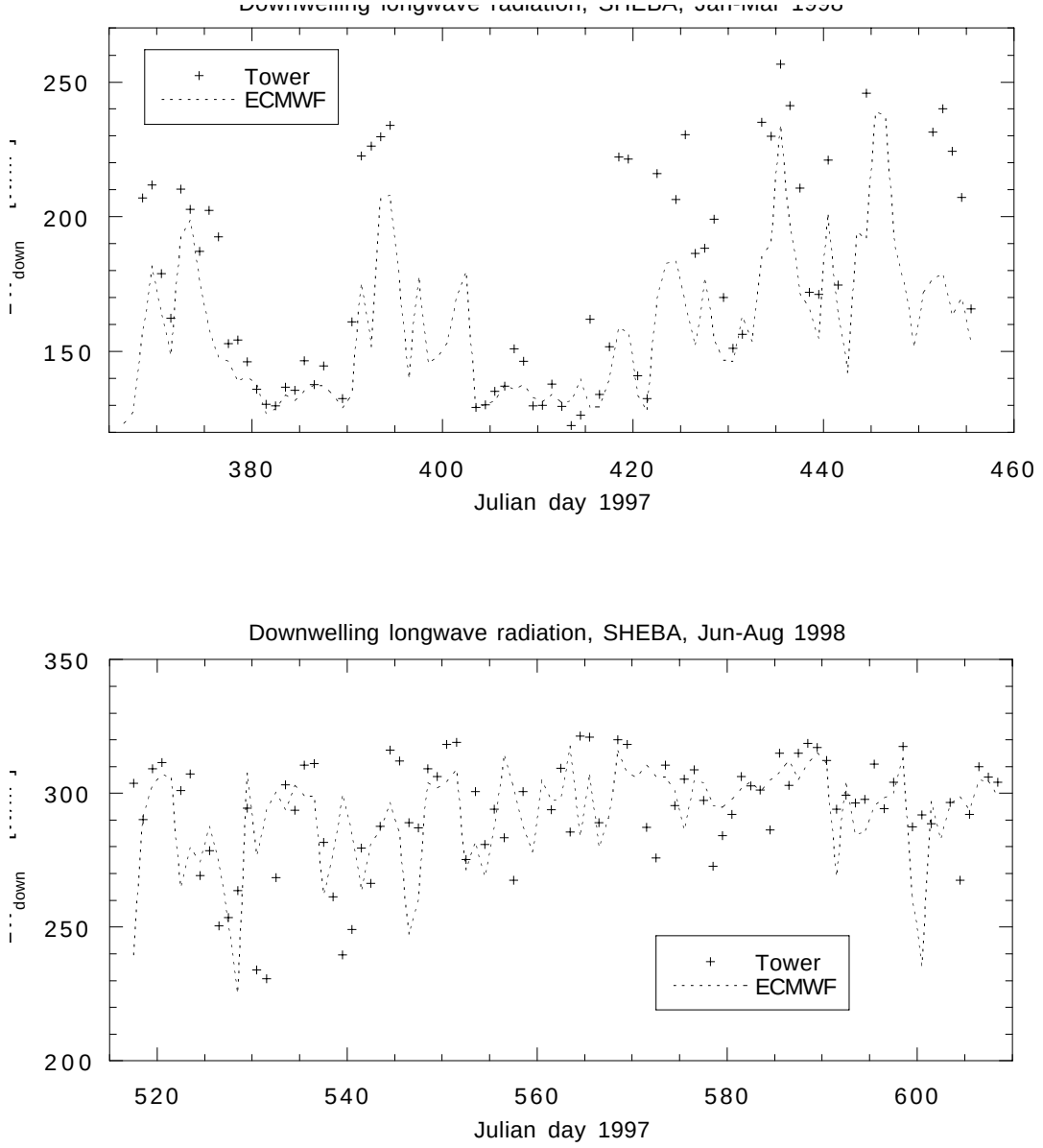

Figure 14. Observed and model-predicted downwelling surface longwave radiation.

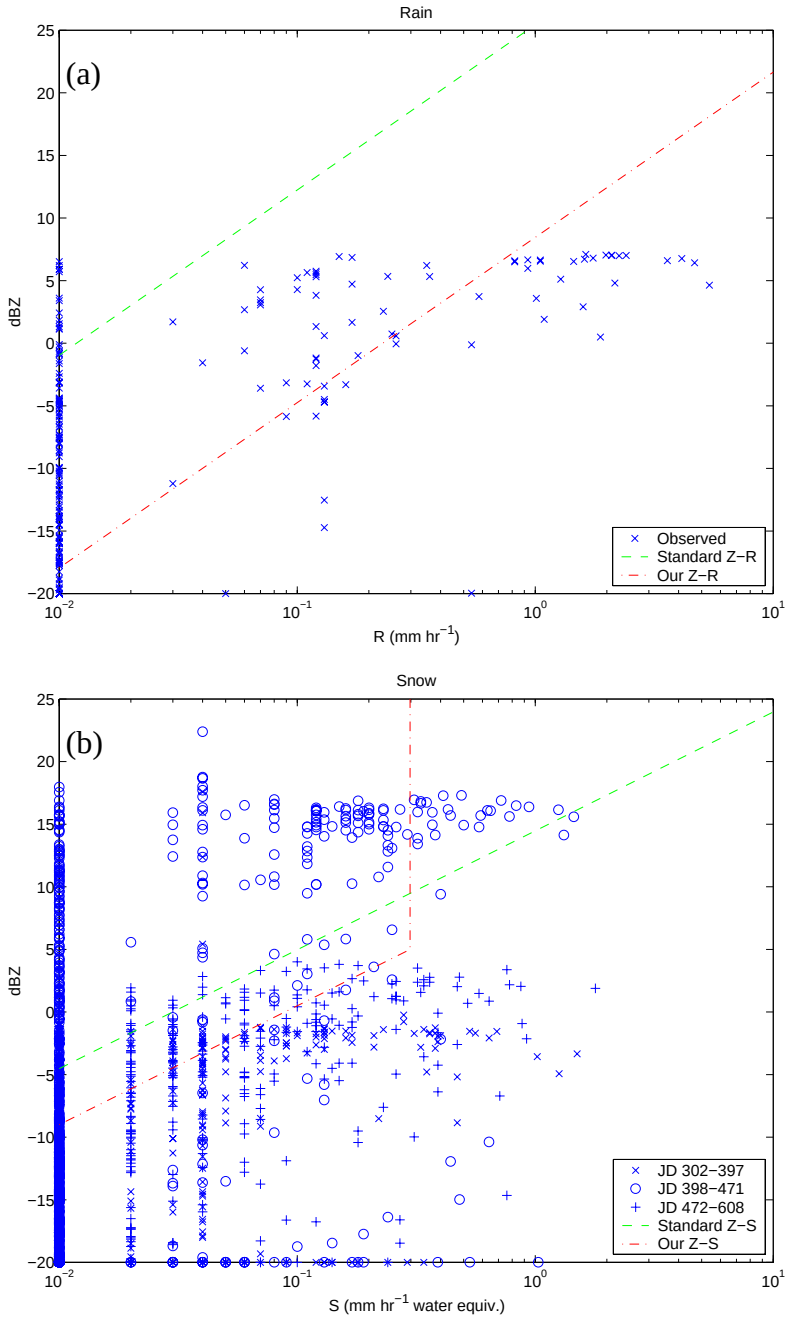

Figure 15. Observed hourly-average reflectivity at 400 m vs. precipitation rate for (a) rain (T > 273 K or mean fall speed > 3 m s^{-1}) and (b) snow (all other times).

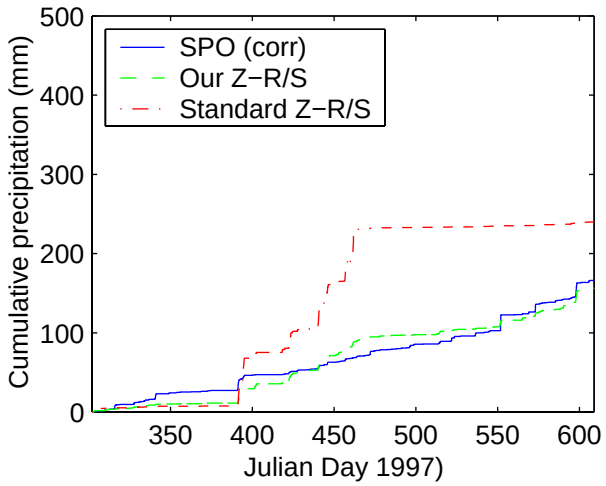

Figure 16. Cumulative precipitation from corrected SPO measurements compared with predictions based on from hourly-average reflectivity at 400 m and two *Z-R/S* relations - our empirical relations (4-5) (using a 5 dBZ reflectivity cap for snowfall) and the standard midlatitude relations (A1-A2)..